

REFERENCES AND NOTES

1. C. Frieden and L. W. Nichol, Eds., *Protein-Protein Interactions* (Wiley, New York, 1981).
2. For example, W. Bode, E. Papamokos, D. Musil, U. Seemuller, H. Fritz, *EMBO J.* **5**, 813 (1986).
3. R. Huber, *Science* **233**, 702 (1986); A. G. Amit, R. A. Mariuzza, S. E. V. Phillips, R. J. Poljak, *ibid.*, p. 747; D. R. Davies, S. Sheriff, E. A. Padlan, *J. Biol. Chem.* **263**, 10541 (1988).
4. T. L. Poulos, S. Sheriff, A. J. Howard, *J. Biol. Chem.* **262**, 13881 (1987).
5. G. W. Pettigrew and G. R. Moore, *Cytochromes c: Biological Aspects* (Springer-Verlag, New York, 1987).
6. B. Guiard and F. Lederer, *J. Mol. Biol.* **135**, 639 (1979).
7. F. S. Mathews and E. W. Czerwinski, in *Enzymes of Biological Membranes*, A. N. Martonosi, Ed. (Plenum, New York, 1976), vol. 4, pp. 143-197; F. S. Mathews, *Prog. Biophys. Mol. Biol.* **45**, 1 (1985).
8. B. Guiard and F. Lederer, *Eur. J. Biochem.* **100**, 441 (1979).
9. K. H. D. Le and F. Lederer, *EMBO J.* **2**, 1909 (1983).
10. D. E. Hultquist and P. G. Passon, *Nature New Biol.* **229**, 252 (1972); L. J. Sannes and D. E. Hultquist, *Biochim. Biophys. Acta* **544**, 547 (1978).
11. A. Ito, *J. Biochem. (Tokyo)* **87**, 63 (1980); *ibid.*, p. 73; F. Lederer, R. Ghirir, B. Guiard, S. Cortial, A. Ito, *Eur. J. Biochem.* **132**, 95 (1983).
12. S. Ng, M. B. Smith, H. T. Smith, F. Millett, *Biochemistry* **16**, 4975 (1977); J. Stonehuerner, J. B. Williams, F. Millett, *ibid.* **18**, 5422 (1979).
13. P. W. Holloway and H. H. Mantsch, *ibid.* **27**, 7991 (1988).
14. K. K. Rodgers *et al.*, *Science* **240**, 1657 (1988).
15. M. R. Mauk, L. S. Reid, A. G. Mauk, *Biochemistry* **21**, 1843 (1982).
16. M. R. Mauk, A. G. Mauk, P. C. Weber, J. M. Matthew, *ibid.* **25**, 6381 (1986).
17. C. G. S. Eley and G. R. Moore, *Biochem. J.* **215**, 11 (1983).
18. F. R. Salemme, *J. Mol. Biol.* **106**, 563 (1976).
19. J. J. Wendoloski, J. B. Matthew, P. C. Weber, F. R. Salemme, *Science* **238**, 794 (1987).
20. R. J. Cristiano and A. W. Steggle [Nucleic Acids Res. **17**, 799 (1989)] reported the sequence of a full-length cDNA clone of bovine liver microsomal cyt b₅ that establishes the identity of residue 11 as Glu, residue 13 as Gln, and residue 57 as Asn [by using the crystallographic numbering system of Mathews and co-workers (7)]. Tryptic peptide sequence analysis of trypsin-solubilized bovine liver microsomal cyt b₅ has recently confirmed the identity of these residues (W. D. Funk, M. R. Mauk, R. T. A. MacGillivray, A. G. Mauk, unpublished results).
21. Model building has made use of both the tuna (18, 19) and simulated horse heart cyt c (16) structures. The close similarity in behavior and structure of these two proteins renders them effectively identical to each other for this purpose.
22. Recent potentiometric titrations demonstrate that the stability of the complex formed by horse heart cyt c is greater for the complex formed with the triple mutant of cyt b₅ than for the complex formed with the true wild-type cyt b₅ (pH 7.2, 25°C, ionic strength = 0.01M (M. R. Mauk, P. D. Barker, A. G. Mauk, unpublished results). Crystallographic analysis of the triple mutant has recently established that it does not exhibit any significant distortion of the main chain conformation relative to wild-type cyt b₅; the principal differences between the two structures involve surface hydrogen-bonding changes in the vicinity of the amino acid substitutions (W. D. Funk *et al.*, in preparation).
23. A. P. Boswell, G. R. Moore, R. J. P. Williams, J. C. W. Chien, I. C. Dickinson, *J. Inorg. Biochem.* **13**, 347 (1980).
24. A. M. Burch *et al.*, *Biochem. Soc. Trans.* **16**, 844 (1988).
25. H. Santos and D. L. Turner, *FEBS Lett.* **194**, 73 (1986).
26. C. J. A. Wallace and D. E. Harris, *Biochem. J.* **217**, 589 (1984); C. J. A. Wallace, *ibid.*, p. 595; G. W. Pettigrew, I. Aviram, A. Schejter, *Biochem. Biophys. Res. Commun.* **68**, 807 (1976).
27. A. P. Boswell *et al.*, *Biochem. J.* **213**, 679 (1983).
28. We discount the possibility that the shifts in the N-acetimidyl methyl peaks result from protein conformational changes induced by complex formation primarily because the shifts of these peaks are larger than for any other amino acid ¹H NMR perturbations induced by complex formation. However, shifts produced by a change in conformation of modified Lys residues that result from the presence of these residues within the protein complex interface region but not involved in salt bridges cannot be excluded on the basis of the NMR data alone. It seems unlikely that a Lys would be in such a position and not be involved in local electrostatic interactions, and, indeed, none of the computer graphics models place a Lys in such a position.
29. Supported by the Science and Engineering Research Council, United Kingdom, under their Molecular Recognition Initiative (G.R.M.), NIH grant GM-28834 (A.G.M.), Medical Research Council of Canada grant MT-10317 (R.T.A.M.), British Columbia Health Care Research Foundation Major Equipment grant 215(87-ME) (A.G.M.), and NATO travel grant 0145/87 (A.G.M. and G.R.M.).

28 August 1989; accepted 30 November 1989

Painting the Phase Space Portrait of an Integrable Dynamical System

SHANNON COFFEY, ANDRÉ DEPRIT, ETIENNE DEPRIT, LIAM HEALY

For an integrable dynamical system with one degree of freedom, "painting" the integral over the phase space proves to be very effective for uncovering the global flow down to minute details. Applied to the main problem in artificial satellite theory, for instance, the technique reveals an intricate configuration of equilibria and bifurcations when the polar component of the angular momentum approaches zero.

SEVERAL DEVELOPMENTS UNDERLIE the present revival in classical mechanics, including computerized algebraic processors and color graphics. Dynamical processes are very hard to detect beneath the surface of the differential equations. It takes a fair amount of tedious algebra to extract, by averaging or by normalization, the essence of the mechanism from the background of short-term fluctuations and unremarkable perturbations. But to the benefit of nonlinear mechanics, computer algebra systems are becoming increasingly sophisticated. Once over the hurdle of tedious calculations, one faces the obstacle of obtaining a global picture for the long-term trends in the system. Color graphics proves invaluable in visualizing the global behavior of the system and in discovering minutiae of local behavior hidden beneath the mass of calculations. Pseudocoloring a function over a domain, a widespread technique in applied mathematics, has produced stunning pictures; they have opened the eyes of mathematicians to hitherto unsuspected phenomena in the dynamics of nonlinear maps (1). Extension to classical mechanics forces a search for refinements in the technique such as the automatic selection of colors to ensure enough contrast around isolated but close singularities.

Here is an example of basic facts discovered by color graphics. It is borrowed from

a problem that has been vexing astronomers and space engineers since Orlov (2) uncovered the singularity of the "critical inclination." Take a point mass in the gravity field of the earth; ignore for the moment all other bodies in the vicinity, the nongravitational forces (drag and radiation pressure), and even those parts of the earth's gravity field that are dependent on the longitude. Furthermore, in the remaining, ignore all zonal harmonics except the one caused by the equatorial bulge. Thus, the system is represented by the Hamiltonian

$$\mathcal{H} = \frac{1}{2}(\mathbf{X} \cdot \mathbf{X}) - \frac{\mu}{r} \left[1 - J_2 \left(\frac{\alpha}{r} \right)^2 P_2 \left(\frac{\mathbf{k} \cdot \mathbf{x}}{r} \right) \right] \quad (1)$$

where the vectors \mathbf{x} and \mathbf{X} stand for the position and velocity of the spacecraft, respectively; $r = \|\mathbf{x}\|$ is the geocentric distance. The parameters of the system are as follows: μ , the product of the gravitational constant and the mass of the earth; α , the equatorial radius of the earth; \mathbf{k} , the direction of the polar axis of the earth; and a dimensionless quantity J_2 . The function P_2 is the Legendre polynomial of degree 2. Hamiltonian Eq. 1 defines the main problem in artificial satellite theory. This dynamical system admits two integrals: (i) the energy \mathcal{H} per unit of mass, because \mathcal{H} is time-invariant, and (ii) the projection $H = \mathbf{k} \cdot \mathbf{G}$ of the angular momentum $\mathbf{G} = \mathbf{x} \times \mathbf{X}$ per unit of mass on the polar axis, because the group of rotations about \mathbf{k} leaves \mathcal{H} invariant. For lack of a third integral in involution with H , the consensus among experts is that the main

S. Coffey, E. Deprit, L. Healy, Naval Center for Space Technology, Naval Research Laboratory, Washington, DC 20375.
A. Deprit, National Institute of Standards and Technology, Gaithersburg, MD 20899.

problem, Eq. 1, of artificial satellite theory is not integrable.

Because J_2 is approximately 10^{-3} for the earth, the main problem may be regarded as a Keplerian system with Hamiltonian

$$\mathcal{H}_0 = \frac{1}{2}(\mathbf{X} \cdot \mathbf{X}) - \frac{\mu}{r} \quad (2)$$

subject to a perturbation derived from the potential

$$J_2 \left(\frac{\mu}{r} \right) \left(\frac{\alpha}{r} \right) P_2 \left(\frac{\mathbf{k} \cdot \mathbf{x}}{r} \right) \quad (3)$$

We restrict ourselves to the domain $\mathcal{H}_0 < 0$ of bounded orbits sufficiently away from the hypersurface where $G = \|\mathbf{G}\| = 0$. In that region of phase space, averaging over the mean anomaly replaces the full model Eq. 1 by an integrable approximation \mathcal{H} expanded as a power series in the small parameter J_2 .

Normalizing \mathcal{H} by averaging is not a simple task by any means. It is so involved, in fact, that general purpose systems for symbolic algebra such as Macsyma, Maple, or Mathematica have yet to meet the challenge. However, with a tool especially designed for carrying the developments typical of celestial mechanics, we produced

$$\mathcal{H} = \sum_{i=0}^{\infty} \frac{1}{i!} J_2^i \mathcal{H}_i \quad (4)$$

to the fourth power in J_2 . The work was first done in FORTRAN on an advanced array processor (3) and was checked a few years later on a powerful Lisp workstation (4). For our purposes, the reader needs to know only about the first three terms in Eq. 4. Expressed in the variables (ℓ, g, h, L, G, H) introduced by Delaunay (5), these terms are (6)

$$\mathcal{H}_0 = -\frac{\mu^2}{2L^2} \quad (5)$$

$$\mathcal{H}_1 = nG \left(\frac{\alpha}{p} \right)^2 \left(\frac{1}{2} - \frac{3}{4}s^2 \right) \quad (6)$$

$$\begin{aligned} \mathcal{H}_2 = \frac{1}{2} nG J_2^2 \left(\frac{\alpha}{p} \right)^4 & \left\{ -\frac{15}{8} + \frac{15}{4}s^2 - \frac{105}{64}s^4 \right. \\ & + \eta \left(-\frac{3}{4} + \frac{9}{4}s^2 - \frac{27}{16}s^4 \right) \\ & + \eta^2 \left(\frac{3}{8} - \frac{3}{8}s^2 - \frac{15}{64}s^4 \right) \\ & + \cos 2g \left[\frac{93}{16}s^2 - \frac{225}{32}s^4 \right. \\ & + (\beta + \eta) \left(-3s^2 + \frac{15}{4}s^4 \right) \\ & \left. \left. + \eta^2 \left(-\frac{21}{16}s^2 + \frac{45}{32}s^4 \right) \right] \right\} \quad (7) \end{aligned}$$

These terms are expressed in the averaged angles (ℓ, g, h) and actions (L, G, H) . The angle ℓ is the mean anomaly; g is the angle between the line of nodes and the semimajor axis; h is the angle between the line of nodes and a fixed direction in the earth equatorial plane. Together with the Keplerian variables a and e , we have introduced the quantities

$$\begin{aligned} n &= \sqrt{\frac{\mu}{a^3}}, p = a(1 - e^2), \\ \eta &= \sqrt{1 - e^2}, \beta = (1 + \eta)^{-1} \quad (8) \end{aligned}$$

Usually one thinks of the variables (a, e, g) as defining an ellipse with semimajor axis a and eccentricity e whose position in its own plane is determined by the angle g of the major axis of symmetry. In these notations, the actions L and G are

$$L = \sqrt{\mu a}, G = L\eta = \sqrt{\mu p} \quad (9)$$

The inclination I of the plane containing ellipses with characteristics (a, e, g) is defined by the relations

$$\cos I = H/G, 0 \leq I \leq \pi \quad (10)$$

where H is the integral of polar angular momentum. To be concise, we set

$$c = \cos I, s = \sin I \quad (11)$$

By virtue of the averaging, L is an integral for Eq. 4. Thus, above each point in the portion of the plane (H, L) where $L > 0$ and $0 \leq |H| \leq L$, the phase space of the averaged main problem constitutes a two-dimensional manifold—the sphere (7)

$$\xi_1^2 + \xi_2^2 + \xi_3^2 = \frac{1}{4}(L^2 - H^2)^2 \quad (12)$$

in the three-dimensional real space defined by the coordinates

$$\begin{aligned} \xi_1 &= LGse \cos g \\ \xi_2 &= LGse \sin g \\ \xi_3 &= G^2 - \frac{1}{2}(L^2 + H^2) \quad (13) \end{aligned}$$

For convenience, we refer to the great circle $\xi_3 = 0$ as the equator of Eq. 12, and to the points $[0, 0, \pm \frac{1}{2}(L^2 - H^2)]$, as the north pole and the south pole, respectively. The argument of perigee g serves as longitude over Eq. 12, whereas G measures essentially the height above the equatorial plane $\xi_3 = 0$. One learns quickly to interpret geometric curves on the sphere defined by Eq. 12 as orbits of the averaged system Eq. 4. For instance, the point where G attains its maximum value L , that is, the north pole of Eq. 12, represents the instantaneous circular orbit of radius a in a plane at an angle $I = \arccos H/L$ over the equator of the earth; likewise, being the point at which G reaches its minimum value H , the south pole

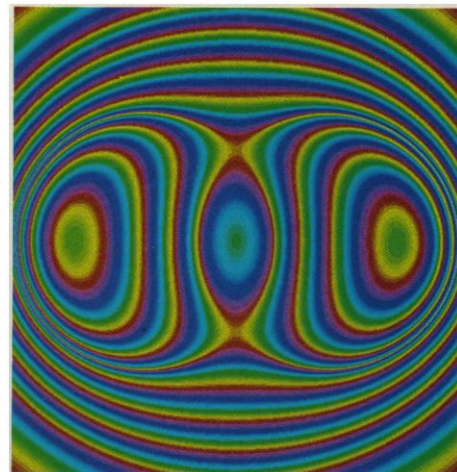


Fig. 1. The phase flow after the second pitchfork bifurcation. A view of the northern cap.

stands for an ellipse with eccentricity $(1 - H^2/L^2)^{1/2}$ in the equatorial plane of the earth.

Because the orbits of the averaged main problem are the level curves of Eq. 4, we get a picture of the phase flow for \mathcal{H} by drawing these level curves for H running over the interval $0 \leq H \leq L$. Now we can think of three methods for drawing the level curves of \mathcal{H} over Eq. 12: method 1, integrating numerically the differential equations

$$\dot{\xi}_i = (\xi_i, \mathcal{H}) \quad \text{for } i = 1, 2, 3 \quad (14)$$

the right-hand member designating the Poisson bracket of ξ_i with the Hamiltonian \mathcal{H} ; method 2, for a given set of values (C, H, L) solving numerically the system made of Eq. 12 and of equation $\mathcal{H} = C$; and method 3, “painting” \mathcal{H} over the sphere.

In method 3, an orthographic projection establishes a 1-1 correspondence

$$\Pi : (u, v) \rightarrow (\xi_1, \xi_2, \xi_3) \quad (15)$$

between pixels within a disk (Δ) on the screen and the points on a hemisphere of Eq. 12. The points at which G is zero being excluded, the averaged Hamiltonian \mathcal{H} is bounded over the sphere. Hence, the values

$$\begin{aligned} m &= \min_{(u, v) \in \Delta} \mathcal{H}[\pi(u, v)] \\ M &= \max_{(u, v) \in \Delta} \mathcal{H}[\pi(u, v)] \quad (16) \end{aligned}$$

are finite, and we can set a 1-1 mapping γ of the real interval $[m, M]$ onto a “rainbow” of colors. By “painting” \mathcal{H} over the sphere we mean to attach to each pixel (u, v) in Δ the corresponding color code $\gamma\{\mathcal{H}[\Pi(u, v)]\}$. That is, the Hamiltonian is computed for each point in phase space corresponding to a point plotted in the projection, and a color is assigned with the assignment based on the interval in which this value falls. In this manner, the level curves of \mathcal{H} on the sphere are represented within Δ by contiguous pix-

els having the same color code.

We have used methods 1 and 2; they proved intolerably long, especially in areas crowded with stable and unstable equilibria. In a related calculation performed by the authors, one integration took 3 days on a workstation-class serial computer with a floating-point accelerator. By contrast, the third method turned out to be most effective for seeing level curves; on a parallel machine it takes on the order of a second.

This simple minded scheme fails to provide enough resolution to enhance fine details in the phase flow. It is not sensitive enough, for instance, to locate a shallow minimum at the foot of a steep maximum. Nevertheless, there are techniques to remedy these difficulties. First, color bin boundaries are assigned nonlinearly so that the range of values displayed as a single color is determined by the relative frequency of those values. For example, one color band might represent Hamiltonian values between 0.0 and 0.01, while another represents values between 1,000 and 10,000, if those ranges contain equal numbers of points. Second, several spectra may be traversed in assigning colors. After all, we are not interested in reading values of \mathcal{H} off the screen. Figuring global phase flows from patterns of color contrast is all that is necessary.

The procedure requires calculating \mathcal{H} at hundreds of thousands of points and ranking these values. This computation is naturally data-parallel, because the Hamiltonian is calculated independently at each point. Massively parallel processors now available complete the task in a matter of seconds for an image of 512 by 512 pixels; by contrast, it takes about 3 hours for a serial Lisp workstation to complete the same task. Speed is a decisive advantage when we draw on this "painting" technique to study the

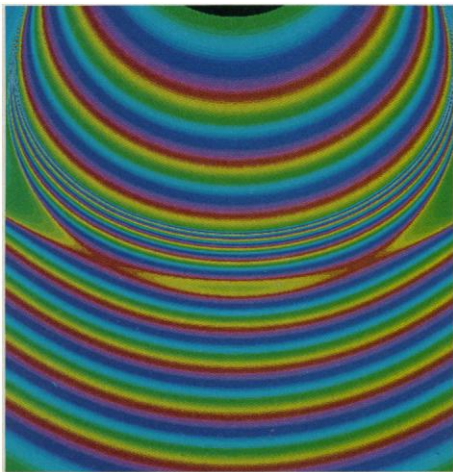


Fig. 2. A surprising bifurcation at E_2 . A zoom into the cover picture.

bifurcation diagram for dynamical systems dependent on one or more parameters. We let the parameters sweep through intervals where we expect a discontinuity in the evolution; for each selection of the parameters, we paint the corresponding Hamiltonian. Comparing successive paintings reveals points in the parameter space where bifurcations occur and provides clues as to their origin.

In the main problem of artificial satellite theory, astronomers and aerospace engineers want to know how the phase flow of the averaged problem evolves as the ratio H/L decreases from 1 (circular orbits in the equatorial plane of the earth) to 0 (orbits residing in a plane passing through the polar axis of the earth).

Because L is an integral after averaging, it is readily seen that the canonical equations derived from Eq. 4 are equivalent to the equations

$$\frac{dg}{dt^*} = \frac{\partial \mathcal{H}^*}{\partial G}, \quad \frac{dG}{dt^*} = -\frac{\partial \mathcal{H}^*}{\partial g} \quad (17)$$

derived from the Hamiltonian

$$\mathcal{H}^* = \mathcal{H}_1 + \frac{1}{2} J_2 \mathcal{H}_2 \quad (18)$$

The independent variable t is replaced by the long time scale t^* such that $dt = J_2 dt^*$. The equilibria in the main problem are the roots of the system

$$\frac{\partial \mathcal{H}^*}{\partial G} = 0, \quad \frac{\partial \mathcal{H}^*}{\partial g} = 0 \quad (19)$$

This system, however, suffers from singularities at $G = L$ (the north pole) and $G = H$ (the south pole); in the neighborhood of these points, it should be replaced by the system

$$\frac{d\xi_i}{dt^*} = (\xi_i, \mathcal{H}^*) \quad \text{for } i = 1, 2, 3 \quad (20)$$

At any point in the interval $0 \leq H \leq L$, system Eq. 20 admits two roots: E_0 at the north pole of the sphere Eq. 12 and E_\mp at the south pole. For all values H/L , the characteristic exponents at E_\mp are imaginary, hence the equilibrium E_\mp is stable. As for E_0 , however, it changes stability twice in the neighborhood of $H = L/\sqrt{5}$. Solving the system Eq. 19 in that neighborhood to the first power of J_2 reveals two discontinuities.

1) A pitchfork bifurcation occurs at

$$H = \left(\frac{L}{\sqrt{5}} \right) \left[1 + \frac{1}{10} J_2 \left(\frac{\alpha}{a} \right)^2 + \mathcal{O}(J_2^2) \right] \quad (21)$$

The north pole becomes unstable while two stable equilibria, $E_1(g = 0, G = G_{1,3})$ and $E_3(g = \pi, G = G_{1,3})$, appear on each side of it with

$$G_{1,3} = H \sqrt{5} \left[1 - \frac{J_2}{250} \left(\frac{L\alpha}{Ha} \right)^4 \right. \\ \left. \times \left(-7 + 20 \frac{H^2}{L^2} + \frac{20H^2/L^2}{1 + H\sqrt{5}/L} \right) \right] + \mathcal{O}(J_2^2) \quad (22)$$

2) A second pitchfork bifurcation occurs at

$$H = \left(\frac{L}{\sqrt{5}} \right) \left[1 - \frac{1}{10} J_2 \left(\frac{\alpha}{a} \right)^2 + \mathcal{O}(J_2^2) \right] \quad (23)$$

At that inclination, E_0 reverts to stability by giving rise to two unstable equilibria, $E_2(g = \pi/2, G = G_{2,4})$ and $E_4(g = -\pi/2, G = G_{2,4})$ with

$$G_{2,4} = H \sqrt{5} \left[1 + \frac{J_2}{500} \left(\frac{L\alpha}{Ha} \right)^4 \right. \\ \left. \times \left(-13 + 7 \frac{H^2}{L^2} + \frac{8H^2/L^2}{1 + H\sqrt{5}/L} \right) \right] + \mathcal{O}(J_2^2) \quad (24)$$

Figure 1 is a painting of the phase flow made at a value of H/L slightly below that of the second bifurcation. It is a view of the northern cap, not of the entire hemisphere, in an orthographic projection from the north pole along the ξ_3 axis. The ξ_1 axis goes from left to right, the ξ_2 axis points upward in the vertical direction.

Most recently, by solving numerically system Eq. 19, Healy found that, for $H/L < 0.031$ (with $J_2 = 0.001$), there appear two more roots for G at $g = 0$ and $g = \pi/2$. They arise as saddle node bifurcations out of a smooth landscape of circulatory flow. There are two pairs of equilibria, one stable E_5 , the other unstable E_6 , located on the positive ξ_1 axis. These equilibria are mirrored by symmetric images (E_7, E_8) on the negative ξ_1 axis. Without the color picture on the cover it would have been very difficult to decipher the pattern of flow around these equilibria because they occur in very shallow areas. The cover picture is an orthographic projection of the south pole after the third pitchfork bifurcation. It shows the discovery of two pairs of saddle node equilibria appearing as eyeballs along the ξ_i axis. The stable equilibrium E_\mp occupies the center; on both sides, one finds first the stable equilibria E_1 and E_3 . Farther away from the center appear the stable equilibria E_5 and E_7 , and then the unstable equilibria E_6 and E_8 . Incidentally, these discoveries stand in contradiction to arguments (8) against the existence of equilibria other than the classical ones at $(E_i)_{0 \leq i \leq 4}$ and E_\mp .

Visual inspection of the painted flow diagrams produced a surprise at the equilibria

E_2 and E_4 . Originally thought to be unstable, E_2 and E_4 appeared unexpectedly as stable points escorted by two unstable equilibria, one on either side of the originals, as seen in Fig. 2. Once again, the ratio H/L passes through a pitchfork bifurcation making E_2 and E_4 stable while spawning pairs of unstable equilibria. After the fact, we found the mathematical explanation. Eliminating G from Eq. 19 produces a quadratic equation in $\sin g$. Previous analysis restricted g to be a multiple of $\pi/2$ to ease the algebraic complexities. Not until the ratio H/L becomes very small does the discriminant of the equation in $\sin g$ become positive, providing for real roots and new equilibria.

We have now come full circle. Analytical study of a dynamical system prompted graphical representations to support our results. Improvements in the visualization techniques revealed new phenomena, which brought us to refine our mathematical analysis.

REFERENCES AND NOTES

1. See, for instance, the cover of *Science*, 30 October 1987, courtesy of C. Grebogi, E. Ott, and J. A. Yorke.
2. A. A. Orlov, *Sobshch. Gos. Astron. Inst. Mosk. Gos. Univ.* **88-89**, 3 (1953); *Tr. Gos. Astron. Inst. Mosk. Gos. Univ.* **24**, 139 (1954).
3. A. Deprit, *J. Guidance Control* **4**, 201 (1981); S. L. Coffey and A. Deprit, *J. Guidance Control Dyn.* **5**, 366 (1982).
4. S. L. Coffey, A. Deprit, E. Deprit, L. Healy, B. R. Miller, in *Proceedings of the Conference on Computer-Aided Proofs in Analysis* (Institute for Mathematics and Its Applications) (Springer-Verlag, New York, in press).
5. C. Delaunay, *C. R. Acad. Sci.* **22**, 32 (1846).
6. S. Coffey, A. Deprit, L. Healy, in preparation; P. Exertier, thèse, Observatoire de Paris (1988).
7. S. L. Coffey, A. Deprit, B. R. Miller, *Celestial Mech.* **39**, 365 (1986).
8. S. Hughes, *ibid.* **25**, 235 (1981).
9. Partial support for this research came from the National Academy of Sciences (as a research associateship for L.H.) and from the Defense Advanced Research Project Agency (to A.D.). Thanks are due to H. Dardy for giving access to the Connection Machine CM-2 at the Naval Research Laboratory. Authors are listed in alphabetical order.

29 August 1989; accepted 20 November 1989

Activin-Binding Protein from Rat Ovary Is Follistatin

TAKANORI NAKAMURA, KOJI TAKIO, YUZURU ETO,
HIROSHIRO SHIBAI, KOITI TITANI, HIROMU SUGINO*

Activin, a member of the transforming growth factor β protein family, was originally isolated from gonadal fluids and stimulates the release of pituitary follicle-stimulating hormone (FSH). Activin has numerous functions in both normal and neoplastic cells. Various cells synthesize activin and have a specific binding site for this peptide. However, the molecular basis for its actions is unknown. A binding protein for activin was purified from rat ovary and was identical to follistatin, a specific inhibitor of FSH release. It is likely that the binding protein participates in the diverse regulatory actions of activin.

SEVERAL HYPOPHYSIOTROPIC PROTEINS that can suppress or enhance follicle-stimulating hormone (FSH) secretion by pituitary cells have been identified from mammalian gonads. These include inhibin (1) and follistatin (2), which inhibit FSH release, and activin (3), which stimulates FSH release. They have potential roles in reproduction and their structures have been elucidated by protein chemistry and cDNA cloning techniques (4, 5).

Activin is a member of the transforming

growth factor β (TGF- β) gene family and may have a variety of similar functions. Activin acts outside the reproductive system as erythroid differentiation factor (EDF). Although EDF was initially isolated from a human leukemia cell line as a protein factor that causes differentiation of erythroid progenitor cells (6), protein chemistry and cDNA cloning analyses of the factor proved that EDF is the same molecular species as activin (7). Activin (EDF) has diverse biological roles: modulation of follicular granulosa cell differentiation (8), regulation of erythropoiesis (9), stimulation of insulin secretion by rat pancreatic islets (10), and modulation of several types of anterior pituitary cells (11). Specific binding sites for activin on rat granulosa cell (12) and human and murine erythroleukemia cells (13) have been identified; activin binding may be responsible for its biological activities. Nevertheless, regulation of the multiple functions

of activin remains obscure.

During our purification of activin receptors we noticed binding proteins for activin in rat ovary homogenates. We therefore

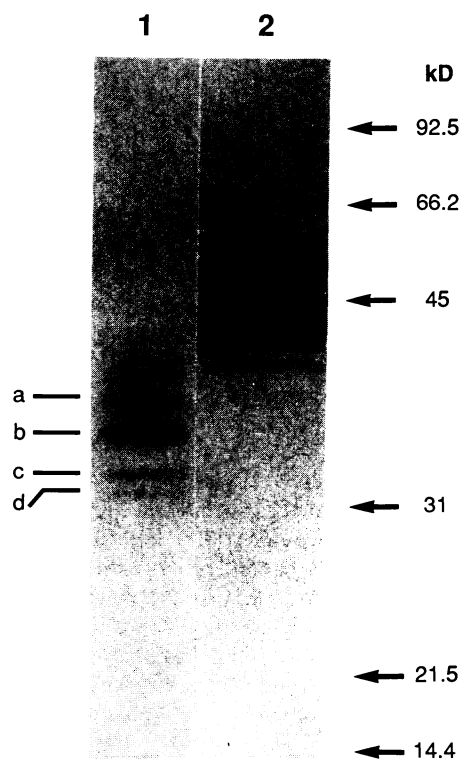


Fig. 1. SDS-PAGE of purified activin-binding protein under nonreducing (lane 1) and reducing (lane 2) conditions. The ovaries (188 ovaries; wet weight, 21 g) were homogenized in 200 ml of Buffer A [20 mM tris-HCl (pH 7.2) with 150 mM NaCl, 5 mM benzamidine-HCl, 1 mM phenylmethylsulfonyl fluoride, 1 mM *N*-ethylmaleimide, 2 mM diisopropylfluorophosphate, 2 mM EDTA, and 20% glycerol] with a Polytron homogenizer. The homogenate was centrifuged; the resulting supernatant was added to an equal volume of Buffer A (with 25% polyethylene glycol 6000 instead of 20% glycerol), stirred for 30 min at 4°C, centrifuged, and the supernatant decanted. The pellet was suspended in Buffer A with Triton X-100 at a final concentration of 2%, stirred, and centrifuged. The supernatant was mixed with the activin-Affi-Gel 10 [5 mg of recombinant activin (EDF) (21) was coupled to 5 ml Affi-Gel 10 (Bio-Rad)] and incubated overnight with a gentle stirring at 4°C. The gel was first washed with 0.1% Triton X-100 in Buffer A and then with 0.1% Triton X-100 in 50 mM sodium acetate buffer (pH 4.0), resuspended in 0.1% Triton X-100 in Buffer A, and poured into a column. Activin-binding protein was eluted with Buffer B (Buffer A with 2M guanidine-HCl and 0.1% Triton X-100). The active fractions desalted by a Bio-Gel P-10 column were applied to an activin-Affi-Gel 10 column, and the column was washed with 0.1% Triton X-100 in Buffer A. The activin-binding protein was eluted with Buffer B. Active fractions were desalted using a Bio-Gel P-10 column equilibrated with 0.001% SDS. SDS-PAGE of the preparation was done in 12.5% gels and proteins were stained with Coomassie brilliant blue (22). Bands a to d identify activin-binding protein.

T. Nakamura, K. Takio, H. Sugino, Frontier Research Program, Institute of Physical and Chemical Research (RIKEN), Wako, Saitama, 351-01, Japan.
Y. Eto and H. Shibai, Central Research Laboratories, Ajinomoto Co., Inc., Kawasaki-ku, Kawasaki, 210, Japan.
K. Titani, Fujita-Gakuen Health University, Toyoake, Aichi, 470-11, Japan and Frontier Research Program, Institute of Physical and Chemical Research (RIKEN), Wako, Saitama, 351-01, Japan.

*To whom correspondence should be addressed.